^{99m}Tc-3P-RGD2 molecular imaging targeting integrin $\alpha_v\beta_3$ in head and neck squamous cancer xenograft

Bing Yan · Fan Qiu · Ling Ren · Haojie Dai · Wei Fang · Haibo Zhu · Feng Wang

Abstract ^{99m}Tc-3P-RGD2 and SPECT/CT were valuable tools for selecting patient likely benefit from integrin $\alpha_v\beta_3$ blocking therapy. To evaluate the feasibility of ^{99m}Tc-3P-RGD2 imaging to detect head and neck squamous cell carcinoma, ^{99m}Tc-3P-RGD2 was prepared and the relationship between its accumulation and integrin $\alpha_v\beta_3$ expression in nude mice bearing HEP-2 or CNE-1 carcinoma xenograft were analyzed. This study demonstrated that ^{99m}Tc-3P-RGD2, with high affinity to integrin $\alpha_v\beta_3$, will provide basis for $\alpha_v\beta_3$ involved individual therapy.

Keywords Head and neck squamous cell carcinoma · Integrin $\alpha_v\beta_3$ · Molecular imaging · ^{99m}Tc-3P-RGD2 · Angiogenesis

B. Yan · L. Ren · H. Dai
Department of Nuclear Medicine, Beijing Tongren Hospital,
Capital Medical University, Beijing 100730, China

F. Qiu · F. Wang (✉)
Department of Nuclear Medicine, Nanjing First Hospital,
Nanjing Medical University, 68 Changle Road, Nanjing 210006,
China
e-mail: fengwangcn@hotmail.com

W. Fang
Cardiovascular Institute & Fu Wai Hospital, Peking Union
Medical College & Chinese Academy of Medical Sciences,
Beijing 100037, China

H. Zhu (✉)
State Key Laboratory of Bioactive Substance and Function of
Natural Medicines, Institute of Materia Medica, Peking Union
Medical College & Chinese Academy of Medical Sciences,
Beijing 100050, China
e-mail: zhuhaibo@imm.ac.cn

Introduction

Head and neck squamous cell carcinoma (HNSCC) was reported as the fifth most common cancer worldwide with high morbidity and low survival [1]. In 2012, about 7,000,000 people have been diagnosed and more than 370,000 died of head and neck cancer, treatment for head and neck squamous cancer is a great challenge worldwide [2]. During 5-year follow-up, the recurrence of patients with advanced cancer is 20–25 % [3, 4]. Second primary cancers occur in 3–5 % of cases per year [5]. Early diagnosis and proper treatment is not only to decrease the morbidity but improve the life quality of patients.

Several imaging were performed for detecting HNSCC, including CT scan, CT perfusion, MRI, MRI perfusion, and ^{18}F-FDG PET/CT. Most HNSCC detected by CT scans were at the advanced stage. MRI has its own limitations, like long scan time, fear of confined spaces. CT perfusion and MRI perfusion could not be use wildly because of the high cost of money. Although ^{18}F-FDG PET/CT is the most commonly used for oncologic purposes, ^{18}F-FDG uptake reflects glucose metabolism and can be observed in several normal tissues with wide variability of the normal pattern influence its power. New effective method is needed.

It is reported that angiogenesis is critical in the development of HNSCC. Several studies have suggested that anti-angiogenesis is important in the prognosis in HNSCC [6–8]. Integrin $\alpha_v\beta_3$, which moderates tumor angiogenesis, specifically binding to arginine–glycine–aspartic acid (RGD) makes RGD a promising tracer to detect tumor and monitor patients receiving anti-angiogenic drugs or $\alpha_v\beta_3$ antagonists [9]. Recently, encouraging results have been achieved with integrin $\alpha_v\beta_3$ antagonists in various malignant tumors [10–12]. The use of etaracizumab [13–15], which is anti-angiogenesis therapy, has been evaluated in

clinical trials. A variety of radiolabeled RGD for single photon emission computed tomography (SPECT) and positron emission tomography (PET) have been developed [16–21]. Nowadays a new radiolabeled tracer, [^{99m}Tc (HYNIC-3P-RGD2)(tricine)(TPPTS)] (^{99m}Tc-3P-RGD2: 6-hydrazinonicotinyl; 3P-RGD2 = PEG4-E[PEG4-c (RGDfK)]2; PEG4 = 15-amino-4,7,10,13-tetraoxapen-tadecanoic acid; and TPPTS = trisodium triphenyl-phosphine-3,3′,3″-trisulfonate), was used in a variety of tumors [22–26]. This study was to evaluate the feasibility of ^{99m}Tc-3P-RGD2 detecting HNSCC in nude mice tumor model and the possibility of choosing proper individual therapy.

Materials and methods

Radiolabeling and quality control

Cyclic RGD peptide 3P-RGD2 was obtained from the School of Health Sciences, Purdue University, USA. Na^{99m}TcO$_4$ was purchased from the Beijing Atom High Tech Co.,Ltd. To a lyophilized vial containing 20 μg of 3P-RGD2 was added 1.0 mL of Na^{99m}TcO$_4$ solution (370–1111 MBq/mL). The vial was heated at 100 °C for 20 min in a lead-shielded water bath. After radio-labeling, the vial was kept at room temperature for 10 min. A sample of the resulting solution was tested by radio-high performance liquid chromatography (HPLC, HP Hewlett Packard Series 1100, USA) at the Peking University Medical Isotopes Research Center. The radiochemical purity was >95 % for ^{99m}Tc -3P-RGD2.

Stability in vitro

The stability of ^{99m}Tc-3P-RGD$_2$ in newborn calf serum was determined after incubating the radiolabeled compound (37 MBq) in 2 mL human serum at 37 °C. Every 20 μL mixture was injected directly into the radio-HPLC to analyze the radiochemistry purity, which was followed by radiolabeling efficiency analysis at 0 min, 3, 4, and 6 h.

Cell culture

Human laryngeal cancer cells HEP-2 and human naso-pharyngeal cancer cells CNE-1 (Cancer Hospital, Chinese Academy of Medical Sciences, China) were maintained at 37 °C and 5 % CO2 in RPMI 1,640 medium containing 10 % fetalbovine serum (FBS).

Western blot

The cells were lysed with cell lysis buffer (150 mmol/L NaCl, 1 % [vol./vol.] Triton X-100, 0.5 % [wt/vol.] sodium

deoxycholate, 0.1 % [wt/vol.] SDS, 50 mmol/L Tris–HCl, pH 7.4) containing protease inhibitor cocktail (Sigma). The lysate was subjected to SDS-PAGE, transferred to poly (vinylidene fluoride) (PVDF) membranes, and incubated with the primary antibodies [rabbit anti human integrin beta3 (Chemicon, Temecula, CA, USA) and mouse anti human beta-actin (Chemicon, Temecula, CA, USA)], followed by horseradish peroxidase-conjugated secondary antibody (Amersham, Little Chalfont, Bucks, UK). The bound antibody was visualised using enhanced chemilu-minescence reagents (Pierce, Rockford, USA). The inte-grated density of each lane was quantified by Image J (Image Processing and Analysis in Java) program.

Animal model

Female BALB/c nude mice (4–5 weeks of age, 15–20 g of weight) were purchased from the Department of Animal Experiment, Chinese Academy of Medical Sciences. The mice were subcutaneously implanted with 3×10^6 the HEP-2 cells (6 mice) or 2×10^5 the CNE-1 cells (6 mice) in 0.1 mL of saline into the right upper shoulder flanks. All procedures were performed in a laminar flow cabinet using the aseptic technique. Fifteen to nineteen days after inoc-ulation, the tumor size was 1–1.5 cm, the tumor-bearing mice were used for biodistribution and imaging studies. Capital Medical University Animal Care and Use Com-mittee approved the animal experiments.

Biodistribution

The biodistribution of ^{99m}Tc-3P-RGD2 in HEP-2 tumor bearing mice and CNE-1 tumor bearing mice was evalu-ated in groups of 3 mice per time point at 60 min and 120 min after injection of approximately 0.55–0.74 MBq of ^{99m}Tc-3P-RGD2 in 0.1 mL saline via tail vein. From all mice, tumors and tissue samples (blood, heart, liver, spleen, kidney, lung, intestine and muscle) were harvested and weighed. Subsequently, radioactivity uptake was deter-mined in γ-counter. Activity concentrations in the tissues were calculated as percentage of the injected dose per gram of tissue (%ID/g). To correct for radioactive decay, injec-tion standards were counted simultaneously.

Whole-body micro single-photon emission computed tomography/computed tomography imaging

SPECT/CT scans and images were obtained with a Micro SPECT/CT PLUS system (Bioscan; Washington DC) equip-ped with a 0.74-mm nine-pinhole collimator: SPECT: 140 keV, 30 s/frame, 256 × 256 matrix, 20 % window; CT scanner: 55 kVp, exposed time: 1,000 ms, 180° plane. Static scans of 12 tumor-bearing mice (6 HEP-2, 6 CNE-1) were

obtained 60 min after tail vein injection of approximately 37–55.5 MBq of ^{99m}Tc-3P-RGD2 in 0.1 mL saline. All 12 mice were anesthetized with 1.5 % isoflurane for micro SPECT/CT and throughout imaging. It took 30 min to complete the whole-body SPECT scan and 15 min to complete the whole body CT scan. SPECT and CT data were reconstructed using InvivoScope software (Bioscan; Washington DC). The volumes of interest were drawn manually to cover the entire tumor. Based on the view in the CT image, the soft, non-tumor tissue reference (in the same trans-axial plane, muscle) was also marked, and the T/NT ratios were calculated.

Immunohistochemical staining

For immunohistochemical investigation, formalin-fixed, paraffin-embedded tumor tissues from mice were sectioned (5 μm) and stained using the biotinylated monoclonal anti-$\alpha_v\beta_3$ antibody (1:100, rabbit IgG; Beijing Biosynthesis Biotechnology, China). The appropriate secondary antibody (Rabbit SP Kit, Beijing Biosynthesis Biotechnology, China) was used. Sections were processed by peroxidase staining (Diaminobenzidine Kit, Beijing Biosynthesis Biotechnology, China).

Light microscopic evaluation of the density of integrin $\alpha_v\beta_3$ was done according to the Fromowitz method [27]. Staining intensity was determined in five adjacent microscopic fields using a $\times 40$ magnifying lens and a $\times 10$ ocular. The staining positivity was graded on a four-point scale: 0 = no staining, 1 = weak, 2 = moderate, and 3 = strong positivity. The percentage of cells at each intensity was graded on a five-point scale: 0 = 0 %, 1 = 1–25 %, 2 = 26–49 %, 3 = 50–80 %, and 4 = >80 %. The overall staining intensity score was calculated as staining positivity score + percentage of cells score.

Statistical analysis

All statistical analyses were done using SPSS 11.5 (SPSS Inc, USA). Data are presented as mean ± SD. The correlation between quantitative parameters was evaluated by linear regression analysis and calculation of Pearson's correlation coefficient. Student t-tests for unpaired data were conducted to determine the significant differences between the groups in the studies of imaging and biodistribution. Statistical significance was defined as a P value < 0.05.

Results

Radiochemical purity of ^{99m}Tc-3P-RGD2

The radiochemical purity of ^{99m}Tc-3P-RGD2 was determined by radio-HPLC. As shown in Fig. 1, the retention time of ^{99m}Tc-3P-RGD was 14.15 min and the radiochemical purity was over 95 % after preparation.

In vitro stability of ^{99m}Tc-3P-RGD2

As shown in Fig. 2, HPLC analysis results for ^{99m}Tc-3P-RGD2 indicated that it was stable in fetal calf serum after incubation for 6 h.

Expression levels of integrin $\alpha_v\beta_3$ in HEP-2 and CNE-1 cells

The expression level of integrin $\alpha_v\beta_3$ was detected in both cell lines. As shown in Fig. 3, integrin $\alpha_v\beta_3$ was expressed higher in HEP-2 cells than in CNE-1 cells.

Biodistribution

The biodistribution of ^{99m}Tc-3P-RGD2 in HEP-2 and CNE-1 tumor models were summarized as Fig. 4. In the HEP-2 model, the tumor uptake of ^{99m}Tc-3P-RGD2 was moderately high (6.25 ± 0.22 %/g) at 60 min p.i., and its tumor washout was relatively high (4.56 ± 0.67 %/g at 120 min p.i.). In the CNE-1 model, the tumor uptake of ^{99m}Tc-3P-RGD2 was relatively low (2.74 ± 0.51 %/g) at 60 min p.i., and its tumor washout was also high (1.69 ± 0.18 %/g at 120 min p.i.). The tumor uptake of ^{99m}Tc-3P-RGD2 in the HEP-2 model was significantly higher than that in the CNE-1 model at 60 or 120 min p.i. (Student t test, t values = 10.92 and 7.17 respectively, all $P < 0.05$). The kidney uptake of ^{99m}Tc-3P-RGD2 was highest in the selected organs, indicating the radiotracer was excreted predominantly via the renal route. The uptake of ^{99m}Tc-3P-RGD2 in blood and muscle was low at 60 min p.i., and its blood or muscle clearance was relatively high. In the HEP-2 and CNE-1 models, its tumor/blood ratios were 6.37 ± 0.68 and 2.49 ± 0.09 respectively at 120 min p.i., and its tumor/muscle ratios were 4.44 ± 0.42 and 1.86 ± 0.07 respectively at 120 min p.i.. The lower distribution in blood and muscle and higher uptake in tumor guarantees ^{99m}Tc-3P-RGD2 as a valuable tracer to monitor cancers.

Uptakes of ^{99m}Tc-3P-RGD2 in HEP-2 and CNE-1 xenografts

Representative whole body scans of HEP-2 and CNE-1 tumor-bearing mice at 3 h after intraperitoneal administration of ^{99m}Tc-3P-RGD2 were shown in Fig. 5. In the HEP-2 tumor models, the tumors appeared clear with high contrast to the contralateral background at 2 h post-

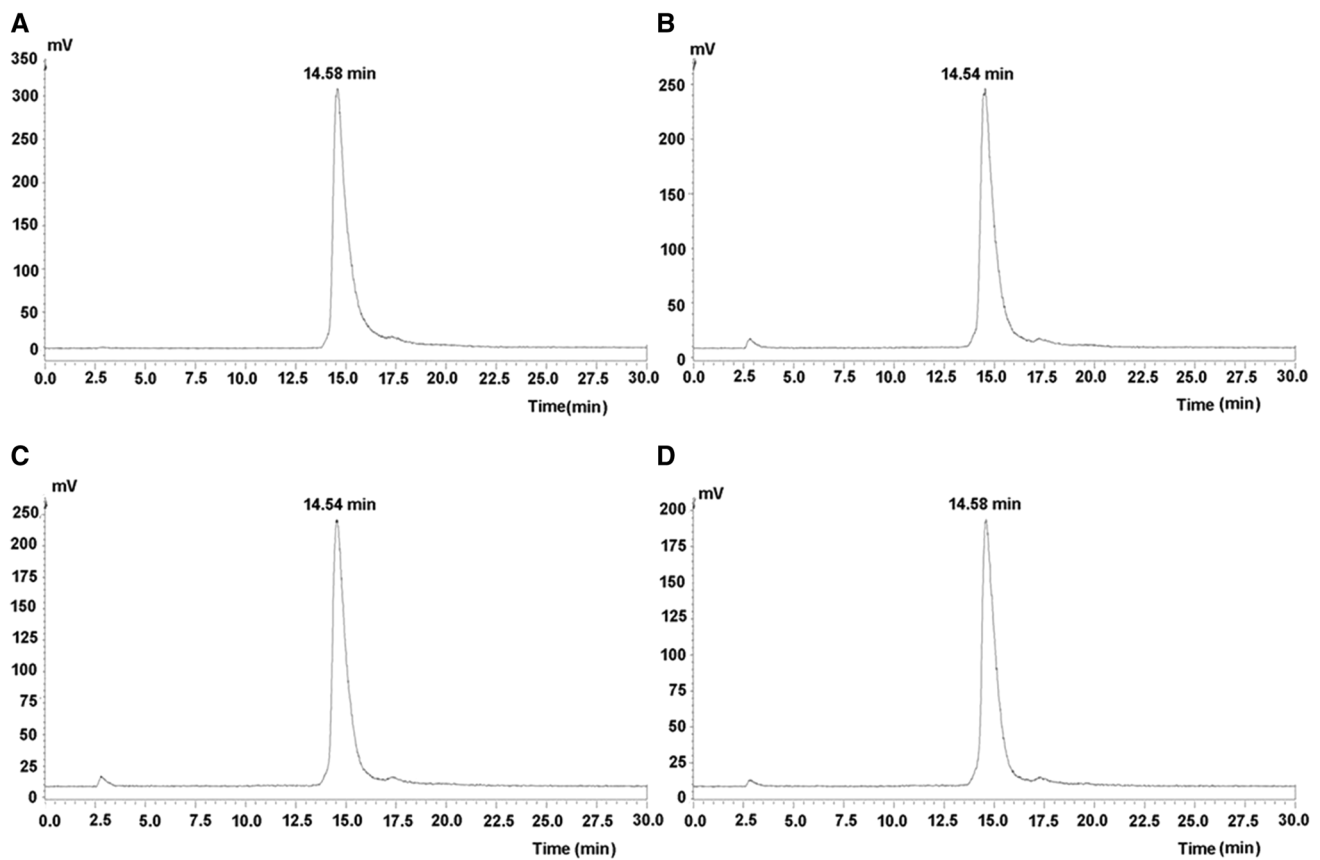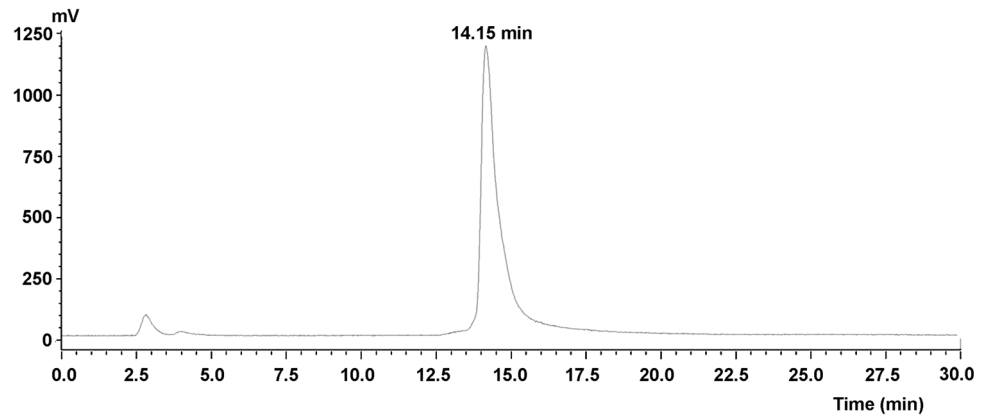**Fig. 1** Radio-HPLC chromatograms for ^{99m}Tc-3P-RGD2

Fig. 2 Radio-HPLC analysis of ^{99m}Tc-3P-RGD2 stability. ^{99m}Tc-3P-RGD$_2$ incubated in new-born calf serum for 0 min (**a**), 3 h (**b**), 4 h (**c**), 6 h (**d**) after labeling

Fig. 3 Integrin $\alpha_v\beta_3$ protein expression in HEP-2 and CNE-1 cells. **a** Western blot analysis for integrinβ_3 expression in HEP-2 and CNE-1 cells and (**b**) quantification for (**a**)
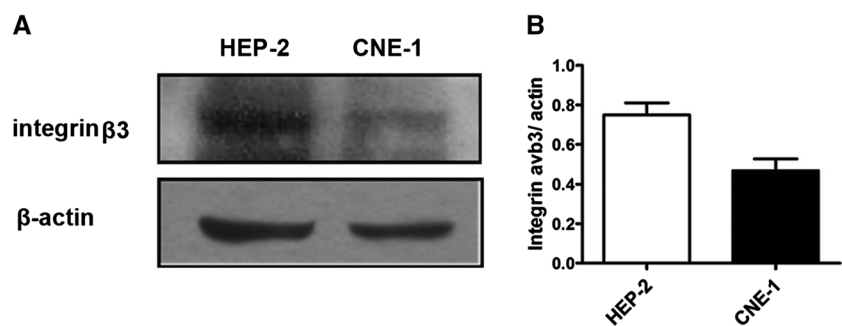
Fig. 4 Biodistribution of ^{99m}Tc-3P-RGD2 in HEP-2 and CNE-1 tumors at 60 or 120 min after tracer injection. Data are mean ± SD
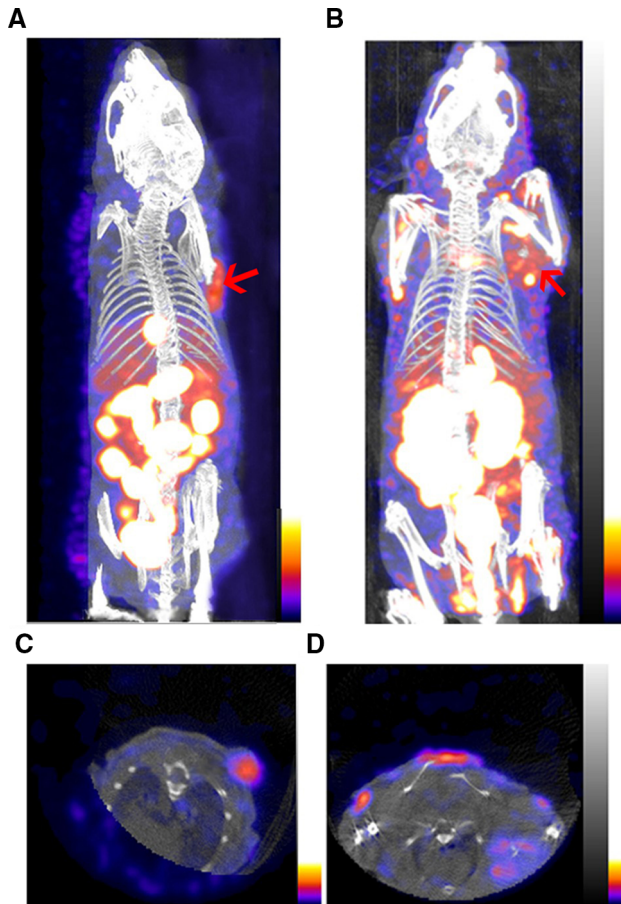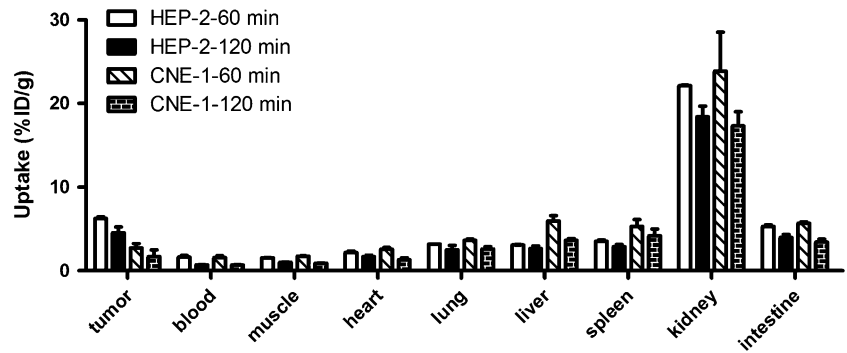

Fig. 5 3D and transverse views of Micro SPECT/CT images of **a** and **c** nude mice bearing HEP-2 tumor and **b** and **d** nude mice bearing CNE-1 tumor 3 h after intravenous injection of ^{99m}Tc-3P-RGD2

injection, and the average T/NT ratio at 3 h was 5.08 ± 0.04. By contrast, in the CNE-1 tumor models, the tumor could be visualized with moderate tumor-to-background contrast at 2 h post-injection with an average T/NT ratio at 3 h of 3.54 ± 0.10. The HEP-2 tumor uptake of ^{99m}Tc-3P-RGD2 was significantly higher than that of CNE-1 tumors ($t = 11.83$, $P < 0.05$).

Integrin $\alpha_v\beta_3$ expression in HEP-2 and CNE-1 tumor tissues

Immunohistochemistry was used to examine the integrin $\alpha_v\beta_3$ expression levels in tumor tissues of different types of head and neck carcinoma, which was quantified by Fromowitz score. The Fromowitz score was 4.97 ± 0.37 in HEP-2 tumor and 2.60 ± 0.36 in CNE-1 tumor respectively. As shown in Fig. 6, integrin $\alpha_v\beta_3$ expression was higher in HEP-2 tumor tissues than in CNE-1 tumor tissues.

Correlation of in vivo uptake of ^{99m}Tc-3P-RGD2 and Integrin $\alpha_v\beta_3$ expression

The uptakes of ^{99m}Tc-3P-RGD2 were correlated well with the expression of integrin $\alpha_v\beta_3$ both in the HEP-2 model (Linear regression analysis, 120 min p.i.: $r = 0.88$, $P < 0.05$; 120 min p.i.: $r = 0.97$, $P < 0.05$), and CNE-1 model (Linear regression analysis, 60 min p.i.: $r = 0.95$, $P < 0.05$; 120 min p.i.: $r = 0.97$, $P < 0.05$).

Discussion

Integrin $\alpha_v\beta_3$ is significantly up-regulated on activated endothelial cells and expresses a lot on various malignant tumor cells, but keep silent on resting endothelial cells or most normal organs [28–32]. Integrin $\alpha_v\beta_3$-targeted RGD provided a molecular imaging way to select high $\alpha_v\beta_3$ express patients and monitor therapy effect of patients receiving anti-angiogenic drugs or $\alpha_v\beta_3$ antagonists.

Radiolabeled RGD tracer should have high affinity and specificity for targeting integrin $\alpha_v\beta_3$. Several strategies have been adopted to improve integin $\alpha_v\beta_3$ binding affinity and specificity of the radiolabeled RGD peptide, such as the use of a multimeric cyclic RGD peptide and insertion of PEG4 spacers in the RGD dimeric molecule [33–35]. ^{99m}Tc-3P-RGD2 has shown faithful effects in detecting
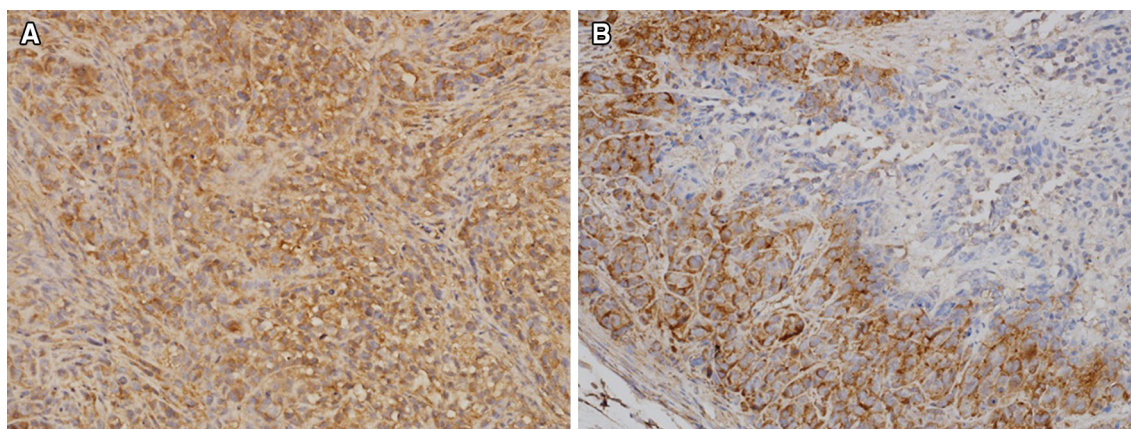
Fig. 6 Immunohistochemical staning of the HEP-2 (**a**) and CNE-1 (**b**) tumor section using the anti-$\alpha_v\beta_3$ monoclonal antibody. The figures demonstrate intense staining predominantly of HEP-2 tumor tissue and circular peripheral staining of CNE-1 tumor tissue ($\times 400$)

carcinoma foci and great advantage in pharmacokinetics. In this study, we evaluated the feasibility of ^{99m}Tc-3P-RGD2 imaging in BALB/c nude mice with HEP-2 and CNE-1 carcinoma xenograft. The results showed that ^{99m}Tc-3P-RGD2 was not only sensitive in detecting the HNSCC foci but highly accumulated in the tumor tissue which was well corresponded with integrin $\alpha_v\beta_3$ expression level.

Our study demonstrated that ^{99m}Tc-3P-RGD2 was excreted predominantly via renal route and lessly evacuated from the hepatobiliary route. The high clearance by kidneys, liver and intestine may minimize the background. However, to detect metastases within or close to kidneys, liver or intestine with this tracer may be limited in clinical practice as reported by previous study that liver metastases could image as hypointense lesions because of high background of ^{18}F-RGD imaging [36]. The uptake of ^{99m}Tc-3P-RGD2 by lung was slightly higher when calculated as ID %/g. However, lung contains much air in vivo, thus, it is reasonable to assume that lung metastases can be visualized clearly with high contrast to normal lung tissue.

Conclusions

Our study demonstrated that the uptake of ^{99m}Tc-3P-RGD2 in HNSCC correlated well with integrin $\alpha_v\beta_3$ expression and ^{99m}Tc-3P-RGD2 SPECT/CT could be used as a non-invasive and effective method for monitoring integrin $\alpha_v\beta_3$ expression in HNSCC for proper patients accept individual therapy.

References

1. Penel N, Amela EY, Mallet Y, Lefebvre D, Clisant S, Kara A et al (2007) A simple predictive model for postoperative mortality after head and neck cancer surgery with opening of mucosa. Oral Oncol 43:174–180
2. Cancer Incidence and Mortality Worldwide: IARC Cancer Base No. 11. Lyon, France: International Agency for esearch on Cancer; 2013. http://globocan.iarc.fr. Accessed 2 May R2014
3. Vermorken JB, Specenier P (2010) Optimal treatment for recurrent/metastatic head and neck cancer. Ann Oncol 21(Suppl 7):vii252–vii261
4. Kearney PL, Watkins JM, Shirai K, Wahlquist AE, Fortney JA, Garrett-Mayer E et al (2011) Salvage resection for isolated local and/or regional failure of head/neck cancer following definitive concurrent chemoradiotherapy case series and review of the literature. McGill J Med 13:29
5. Lee DH, Roh J-L, Baek S, Jung JH, Choi S-H, Nam SY et al (2013) Second cancer incidence, risk factor, and specific mortality in head and neck squamous cell carcinoma. Otolaryngol Head Neck Surg 149:579–586
6. Zätterström UK, Brun E, Willén R, Kjellén E, Wennerberg J (1995) Tumor angiogenesis and prognosis in squamous cell carcinoma of the head and neck. Head Neck 17:312–318
7. O-charoenrat P, Rhys-Evans P, Eccles SA (2001) Expression of vascular endothelial growth factor family members in head and neck squamous cell carcinoma correlates with lymph node metastasis. Cancer 92:556–568
8. Erovic BM, Neuchrist C, Berger U, El-Rabadi K, Burian M (2005) Quantitation of microvessel density in squamous cell carcinoma of the head and neck by computeraided image analysis. Wien Klin Wochenschr 117:53–57
9. Ruoslahti E, Pierschbacher MD (1986) Arg-Gly-Asp: a versatile cell recognition signal. Cell 44:517–518
10. Matter A (2001) Tumor angiogenesis as a therapeutic target. Drug Discov Today 6:1005–1024

11. Longo R, Sarmiento R, Fanelli M, Capaccetti B, Gattuso D, Gasparini G (2002) Anti-angiogenic therapy: rationale, challenges and clinical studies. Angiogenesis 5:237–256

12. Danhier F, Le Breton A, Préat V (2012) RGD-based strategies to target alpha(v) beta(3) integrin in cancer therapy and diagnosis. Mol Pharm 9:2961–2973

13. Moschos SJ, Sander CA, Wang W, Reppert SL, Drogowski LM, Jukic DM et al (2010) Pharmacodynamic (phase 0) study using etaracizumab in advanced melanoma. J Immunother 33:316–325

14. Delbaldo C, Raymond E, Vera K, Hammershaimb L, Kaucic K, Lozahic S et al (2008) Phase I and pharmacokinetic study of etaracizumab (Abegrin), a humanized monoclonal antibody against alphavbeta3 integrin receptor, in patients with advanced solid tumors. Invest New Drugs 26:35–43

15. Hersey P, Sosman J, O'Day S, Richards J, Bedikian A, Gonzalez R et al (2010) A randomized phase 2 study of etaracizumab, a monoclonal antibody against integrin alpha (v) beta3, ±dacarbazine in patients with stage IV metastatic melanoma. Cancer 116:1526–1534

16. Lu X, Wang RF (2012) A concise review of current radiopharmaceuticals in tumor angiogenesis imaging. Curr Pharm Des 18:1032–1040

17. Tateishi U, Oka T, Inoue T (2012) Radiolabeled RGD peptides as integrin alpha(v)beta3-targeted PET tracers. Curr Med Chem 19:3301–3309

18. Gaertner FC, Kessler H, Wester HJ, Schwaiger M, Beer AJ (2012) Radiolabelled RGD peptides for imaging and therapy. Eur J Nucl Med Mol Imaging 39(Suppl 1):S126–S138

19. Cai H, Conti PS (2013) RGD-based PET tracers for imaging receptor integrin $\alpha v \beta 3$ expression. J Label Comp Radiopharm 56:264–279

20. Liu Z, Wang F (2013) Development of RGD-based radiotracers for tumor imaging and therapy: translating from bench to bedside. Curr Mol Med 13:1487–1505

21. Haubner R, Maschauer S, Prante O (2014) PET radiopharmaceuticals for imaging integrin expression: tracers in clinical studies and recent developments. Biomed Res Int. doi:10.1155/2014/871609

22. Zhou Y, Kim YS, Chakraborty S, Shi J, Gao H, Liu S (2011) ^{99m}Tc-labeled cyclic RGD peptides for noninvasive monitoring of tumor integrin $\alpha_V \beta_3$ expression. Mol Imaging 10:386–397

23. Ma Q, Ji B, Jia B et al (2011) Differential diagnosis of solitary pulmonary nodules using ^{99m}Tc-3P4-RGD2 scintigraphy. Eur J Nucl Med Mol Imaging 38:2145–2152

24. Jia B, Liu Z, Zhu Z et al (2011) Blood clearance kinetics, biodistribution, and radiation dosimetry of a kit-formulated integrin $\alpha_V \beta_3$-selective radiotracer ^{99m}Tc-3PRGD2 in non-human primates. Mol Imaging Biol. 13:730–736

25. Zhu ZH, Miao WB, Li QW et al (2012) ^{99m}Tc-3PRGD2 for integrin receptor imaging of lung cancer: a multicenter study. J Nucl Med 53:716–722

26. Zhao D, Jin X, Li F, Liang J, Lin Y (2012) Integrin $\alpha_V \beta_3$ imaging of radioactive iodine-refractory thyroid cancer using ^{99m}Tc-3PRGD2. J Nucl Med 53:1872–1877

27. Fromowitz FB, Viola MV, Chao S, Oravez S, Mishriki Y, Finkel G et al (1987) Ras P21 expression in the progression of breast cancer. Hum Pathol 18:1268–1275

28. Felding-Habermann B (2003) Integrin adhesion receptors in tumor metastasis. Clin Exp Metastasis 20:203–213

29. Brooks PC, Montgomery AM, Rosenfeld M, Reisfeld RA, Hu T, Klier G et al (1994) Integrin alpha v beta 3 antagonists promote tumor regression by inducing apoptosis of angiogenic blood vessels. Cell 79:1157–1164

30. Brooks PC, Clark RA, Cheresh DA (1994) Requirement of vascular integrin alpha v beta 3 for angiogenesis. Science 264:569–571

31. Hood JD, Cheresh DA (2002) Role of integrins in cell invasion and migration. Nat Rev Cancer 2:91–100

32. Ruoslahti E (2002) Specialization of tumour vasculature. Nat Rev Cancer 2:83–90

33. Janssen M, Oyen WJ, Massuger LF, Frielink C, Dijkgraaf I, Edwards DS et al (2002) Comparison of a monomeric and dimeric radiolabeled RGD-peptide for tumor targeting. Cancer Biother Radiopharm 17:641–646

34. Liu S (2009) Radiolabeled cyclic RGD peptides as integrin alpha (v) beta (3)-targeted radiotracers: maximizing binding affinity via bivalency. Bioconjug Chem 20:2199–2213

35. Ji S, Czerwinski A, Zhou Y, Shao G, Valenzuela F, Sowinski P et al (2013) ^{99m}Tc-Galacto-RGD2: a novel ^{99m}Tc-Labeled cyclic RGD peptide dimer useful for tumor imaging. Mol Pharm 10:3304–3314

36. Kenny LM, Coombes RC, Oulie I, Contractor KB, Miller M, Spinks TJ et al (2008) Phase I trial of the positron-emitting Arg-Gly-Asp (RGD) peptide radioligand ^{18}F-AH111585 in breast cancer patients. J Nucl Med 49:879–886